The Effect of Dynamic Normal Force on the Stick-slip Vibration Characteristics

Y.G. Zhu
Southwest Jiaotong University
R.L. Wang
Southwest Jiaotong University
Z.Y. Xiang
Southwest Jiaotong University
Jiliang Mo (jlmo@swjtu.cn)
Southwest Jiaotong University
H. Ouyang
Southwest Jiaotong University

Research Article

Keywords: Single-degree-of-freedom model, Stick-slip, Alternating normal force, Vibration characteristics

Posted Date: April 5th, 2022

DOI: https://doi.org/10.21203/rs.3.rs-1199501/v1

Abstract

In the experiment, we observed such a phenomenon: the alternating normal force changes the vibration state of a friction system. A single-degree-of-freedom mathematical model was used in this paper to discuss the effects of a constant and alternating normal force on the stick-slip vibration characteristics for different dynamic and static friction coefficients. Under the condition that the applied constant normal force continues to increase, the vibration amplitude of the system, the amplitude of the limit cycle, and the adhesion time of the system increase. When the difference between the dynamic and static friction coefficients (DSFC) is small, the system has a complete and clear limit cycle. When the dynamic friction coefficient is reduced, the difference between DSFC increases, and the limit cycle of the system is deformed. The friction system has more abundant dynamic vibration characteristics under an alternating normal force than a constant normal force. The vibration state of the system presents a single-cycle stick-slip vibration when the alternating normal force excites the multi-order harmonic response of the friction system, and the excitation frequency of the alternating normal force is the same as the main response frequency of the system with the highest energy or the low-order even-order main frequency. In contrast, the system exhibits various vibration modes when the excitation frequency of the alternating normal force is dissimilar to the main frequency of the system's highest energy response or is consistent with the odd-order main frequency. In addition, increasing the difference between DSFC or using very high excitation frequencies and excitation amplitudes increase the likelihood of the system entering a chaotic vibration state.

1 Introduction

Friction-induced vibration (FIV) is a common phenomenon in mechanical systems containing friction pairs or contact pairs, such as automobile or rail braking systems, machine tool chip systems, and gear transmission systems [1, 2]. In most cases, FIV has adverse effects, such as increasing the instability of the mechanical system, shortening the service life of parts, altering the friction contact interface, and increasing the risk of fatigue fractures of parts [3–5]. In addition, frictional vibration typically causes friction noise, such as car braking noise, resulting in noise pollution [6–9]. For this reason, many scholars researched the generation and evolution of FIV and have obtained meaningful results [10–13].

In recent years, some scholars have proposed physical mechanisms to explain FIV, such as stick-slip instability [14], the Stribeck negative slope effect [15, 16], and modal coupling [17–20]. These mechanisms can explain FIV in a certain frequency range or under certain conditions; however, no single theory can reasonably and comprehensively explain all FIV phenomena. As a vibration phenomenon with significant nonlinear characteristics, stick-slip is an important aspect of FIV [21]. The main reason for stick-slip vibration is the difference between DSFC of the friction system [22] since two motion states exist: adhesion and sliding. The relative motion speed between two contacting objects in the friction system is zero during adhesion, whereas relative motion exists between the two objects during sliding [23]. Stick-slip vibration can have positive effects, i.e., the stick-slip vibration of a string instrument can produce beautiful music [24], or a friction damper can help reduce vibration [25]. However, stick-slip

vibration typically has adverse effects, such as the groaning noise of a brake system [26, 27] and the damage and crack propagation of the drill of a drilling platform [28–30]. On a larger scale, stick-slip vibration may cause earthquakes and other geological disasters [31, 32]. Thence, it is necessary to carry out research on stick-slip phenomenon and determine the factors that produce and affect stick-slip.

In recent years, researchers have used different methods to study the stick-slip phenomenon. Popp et al. [33] used a discrete model with low degrees of freedom (DoF) and discovered the potential bifurcation and chaos of the stick-slip system. Velde et al. [34] proposed a mathematical model of the stick-slip phenomenon caused by deceleration. They verified that deceleration motion caused stick-slip and analyzed the influence of different parameter combinations, e.g., the damping coefficient, deceleration, stiffness, on predicting the occurrence of stick-slip. Ozaki et al. [35] carried out a numerical analysis of stick-slip instability using a single-DoF model. The authors verified that a change in the friction coefficient had a substantial impact on stick-slip instability and discussed the system's dynamic characteristics, such as the quality, stiffness, and driving speed. Elmaian et al. [36] proposed a three-degree-of-freedom model for characterizing vibration and noise caused by stick-slip, wedge-slip, and modal coupling. By controlling the system parameters, a single model could describe all distinct vibration and noise behaviors. Li et al. [37] used the mass-damper-spring system to study the influence of the lateral runout of the elastic disk on the in-plane stick-slip vibration characteristics. Numerical simulation results showed that the contact separation of the disk and the slider significantly affected the stick-slip vibration and exhibited nonlinear dynamic behavior. Pascal et al. [38] established a two-DoF model considering dry friction and harmonic loads and discussed the stability of the three motion trajectories. Wei et al. [39] constructed a dynamic model of a two-layer braking system to determine the deep reasons for reducing vibration and noise and stick-slip vibration characteristics.

In addition to analyzing stick-slip phenomena using theoretical models with various degrees of freedom, some scholars also carried out experimental studies. Lee et al. [40] experimentally investigated the effects of tangential contact stiffness, volume stiffness, relative sliding velocity, and the difference between DSFC on the intensity and frequency of stick-slip. The test results showed that the intensity and frequency of stick-slip during low-speed braking were substantially affected by all factors. Chandiramani et al. [41] studied the stick-slip phenomenon for various excitation frequencies using the friction wedge damper model and found that the stick-slip phenomenon always occurred around 30 Hz. Park et al. [42] investigated the influence of the brake disc on the stick-slip phenomenon in the case of corrosion. The experimental results showed that the friction film on the material surface enhanced the surface contact rigidity and worsened the stick-slip instability under humid conditions. Under relatively low pressure, this phenomenon is more obvious. Dong et al. [43] assessed the relationship between the polymer's lubrication performance and stick-slip and frictional noise; it was found that materials with better hydrophilicity, self-lubricity, and viscoelasticity produced less stick-slip and lower friction noise. Wang et al. [44] experimentally analyzed the influence of different damping alloys as friction pair materials on stick-slip vibration; the results showed that Mn-Cu damping alloys and aluminum alloys provided the best suppression of stick-slip oscillations. The study also revealed different wear behaviors and clarified the correlation between different wear behaviors and the stick-slip oscillations. Fuadi et al. [45] investigated

the impact of structural stiffness and contact stiffness on stick-slip and categorized the stick-slip motion into three regions: no stick-slip motion, transition zone, and stick-slip motion zone.

Researchers have discussed the stick-slip vibration mechanism and the influence of various factors on stick-slip vibration using theoretical analyses and experimental studies. However, most of these studies used the ideal state of the friction system variables, whereas the parameters change in real time under actual working conditions. For example, the external load of the friction system changes dynamically [46]. Simplifying the variables to the ideal state is convenient for research, and the results are more consistent. However, the conclusions are only suitable for guiding theoretical research and may not be applicable to practical conditions. The normal force is the excitation input of stick-slip vibration and has a crucial influence on the vibration characteristics [47, 48]; any slight changes may cause changes in the vibration characteristics. Krallis et al. [49], Papangelo et al. [50] and Pasternak et al. [51] investigated the impact of changing normal forces on the friction system. To expand, Krallis et al. [49] and Papangelo et al. [50] discussed the critical conditions for the transition between general sliding friction vibration and stick-slip vibration of the friction system on the basis of keeping the static friction coefficient equal to the dynamic friction coefficient. And the influence of parameters such as the amplitude and frequency of the normal force on the critical conditions for the transition of these two states was studied. Pasternak et al. [51] were more inclined to explore how to apply alternating normal forces to eliminate or reduce stick-slip vibration, that is, to change from a stick-slip vibration state to a general sliding friction state. The scope of these three papers is between the general sliding friction vibration state and the stick-slip vibration state, and does not consider that the application of alternating normal force will cause the stick-slip vibration to evolve into a more complex vibration of multiple vibrations state and chaotic vibration state.

Few studies have reported the stick-slip vibration characteristics of friction systems under dynamic loads. Therefore, research on the influence and mechanism of an alternating normal force on the stick-slip vibration characteristics can provide theoretical support and guidance for minimizing the damage caused by stick-slip vibration under actual working conditions. Therefore, this paper uses a discrete mathematical model to investigate the effect of real-time varying dynamic loads and different friction coefficients on the stick-slip vibration characteristics. The results are compared with the stick-slip vibration behavior of a system under a constant force. The dynamic load is designed as a normal force that changes according to the sine law, and different amplitudes and frequencies of the normal force are evaluated in the simulation. The time-domain and frequency-domain characteristics of the stick-slip vibration of the friction system under an alternating normal force are evaluated using bifurcation diagrams, phase-space diagrams, spectrograms, and Poincaré diagrams for different excitation amplitudes and excitation angle frequencies to determine the potential vibration states of the system.

2 Single-degree-of-freedom Mathematical Model

This paper uses the classic undamped single-DoF mass-conveyor belt model to analyze the influence of the alternating normal force on stick-slip vibration. A qualitative analysis is carried out of the dynamic characteristics of the system's stick-slip vibration under an alternating normal force. In the mathematical

model, the friction disc of the test bench in Fig. 1 is simplified as a rigid conveyor belt, and the friction block, clamps, and the buffer part of the test bench are simplified as a mass m. The horizontal spring k_1 represents the constraint of the mass in the tangential direction, as shown in Fig. 2. The mass is simultaneously subjected to the normal force F_N and the frictional force between the rigid belt and the mass moving at a constant speed. It is assumed that the mass and the conveyor belt remain in contact without separation. Since this article focuses on the influence of the alternating normal force on the stick-slip vibration performance of the friction system, the basic parameters in the single-DoF model are set to constants (m = 1 kg, k_1 = 1 N/m, v_0 = 1 mm/s) except the normal loading force F_N. The parameters were selected based on theoretical research [33]. The Coulomb friction model with constant dynamic and static friction coefficients is used to determine the influence of the alternating normal force on the stick-slip motion. Among various influencing factors, the friction coefficient has the most considerable effect on the vibration behavior [41, 42, 52]. Since it is impossible to evaluate if the friction coefficient has a considerable effect on the vibration behavior of the system under an alternating normal force, we select two groups of dynamic and static friction coefficients. The first group includes the static friction coefficient μ_s = 0.4 and the dynamic friction coefficient μ_k = 0.2; the second group consists of the static friction coefficient u_s=0.4 and the dynamic friction coefficient μ_k = 0.1. The simulation calculation is conducted using MATLAB software. The influences of the excitation amplitude (F_ω) and the excitation angular frequency (μ) of the alternating normal force on the stick-slip vibration are investigated.

According to Newton's second law, the dynamic equation of a single-DoF system in the x-direction is expressed as:

$$m\ddot{x}+k_1x=F_f$$

1

The friction force F_f is the product of the friction coefficient and the normal contact force F_N between the mass m and the conveyor belt, where $F_f = \mu F_N$

$$F_N = F_0 + F_\omega \sin(\omega t)$$

2

The ode45 solver in MATLAB is used to solve the time-domain response signal of the system. Due to the interface stick-slip dynamic behavior of the system, the switch model algorithm [53] is used to solve the response of the non-smooth system. It is assumed that the relative speed between the mass block and the conveyor belt is v_r; and its expression is shown in Eq. (3):

$$v_r = v_0 - \dot{x}$$

3

If $\left|v_r\right| > \varsigma$, where ς is the set minimum error value (10^{-6}), relative sliding occurs between the friction block and the conveyor belt, and the system is in the slip state. The expression of the dynamic friction force F_{f-slip} is shown in Eq. (4):

$$F_{f-slip} = \mu_k F_N$$

4

If $\left|v_r\right| < \varsigma$, the friction block and the conveyor belt remain relatively static, and the friction system is in the stick state. The static friction force $F_{f-stick}$ is the combination of the spring force and the maximum static friction force $F_{mf-stick}$. Two conditions can occur, as shown in Eq. (5):

$$F_{f-stick} = \{ {k_1 x \ \ Spring\ force \leqslant}$$

5

3 Test Equipment, Results And Discussion

3.1 Test equipment and parameters

The experiment is conducted on the CETR-UMT-3 multifunctional friction and wear testing machine using a typical pin-disk surface contact mode. The equipment consists of a test device and a signal acquisition device. The friction block sample and the friction disk sample are attached to the test device with a friction block clamp and friction disk clamp, respectively. The friction block consists of composite material, with dimensions of 9 mm × 9 mm × 15 mm and roughness of 0.4 μm. The friction disc is forged steel with a diameter of 25 mm, a thickness of 3 mm, and roughness of 0.06 μm. The friction radius between the friction block and the friction disc, i.e., the distance between the two components, is 6.1 mm. The normal force and friction force during the test are measured by the built-in two-dimensional force sensor (sensitiveness: 0.025 N; range: 5 ~ 500 N) inside the CETR, and the data are stored in the computer that controls the CETR machine. The tangential vibration velocity of the friction block is measured by a laser vibrometer (model: Polytec PDV-100; sensitivity: 8 mv/mm/s; range: ±500 mm/s; frequency response: 0.5 ~ 22 kHz). The measured data are collected by an 8-channel data acquisition instrument (DH5922N), and the sampling frequency is 10 kHz. The normal, tangential, and radial vibration acceleration signals of the friction block are measured by a three-dimensional acceleration sensor (model: KISTLER 8688A50; sensitiveness: 100 mV/g; frequency response: 0.5 ~ 5 kHz), and the measured data are collected by the 8-channel data acquisition instrument; the sampling frequency is 10 kHz. The test is conducted in a dry environment under standard atmospheric pressure (room temperature: 24 ~ 27°C; relative humidity: 60 ± 10%).

The test is divided into two parts. First, a constant normal force of 160 N, 180 N, and 200 N is applied. Second, an alternating normal force is applied with the following parameters: median force F_0 = 180 N,

amplitude F_{ω}=20 N, and excitation frequencies of 0.25 Hz, 0.5 Hz, 1 Hz, and 2 Hz (the relationship between the excitation frequency f and the excitation angular frequency ω is: $f = \omega/2\pi$).In the process of test, the rotation speed of the friction disc remains constant at 2.5 rpm, the duration of each group of tests is 2 minutes, and each set of tests is repeated 3 times.

3.2 Test results and discussion

The tangential velocity signal measured by the laser vibrometer is integrated in the frequency domain to obtain the tangential displacement signal. Figure 3 shows the phase diagrams of the system in the stable phase of 50 s-52 s under three constant normal forces. The velocity in the stick stage is not constant, but there are slight fluctuations due to the inevitable jitter of the test equipment during the test. Under the condition that the applied constant normal force continues to increase, the displacement of the system in the stick state increases. After the displacement reaches the maximum value, it decreases, and with the rapid decrease in speed, the displacement increases rapidly. Since the rotation speed of the friction disc is constant, the greater the normal force, the greater the frictional force of the friction interface is. Thus, the system must accumulate more tangential elastic potential energy to overcome the frictional force. Therefore, since the maximum static friction of the interface was not been exceed by the elastic potential energy, the tangential displacement of the system continues to increase, and more kinetic energy is accumulated for release in the slip phase. As a result, the speed amplitude of the system increases in the slip phase, corresponding to an increase in the amplitude of the middle limit cycle, as shown in Fig. 3.

Figure 4 shows the tangential vibration acceleration signal and the root mean square (RMS) value of the system in the stable phase of 50 s-52 s under the constant normal force. The tangential acceleration signal of the system exhibits periodic relatively constant values and peaks. When the acceleration is zero, the friction block and the friction disc are in a relatively static state, and a sudden change in acceleration means that the friction block and the friction disc are in a sliding state. Under the constant normal force, the acceleration amplitude depends on the magnitude of the applied normal force. The greater the applied normal force, the greater the acceleration amplitude is, i.e., the system is transitioning to a more intense stick-slip vibration state. The acceleration RMS increases with an increase in the normal force.

Figure 5 exhibits the phase diagram in the stable phase of 50 s-55 s under the four alternating normal forces. The amplitude of the limit cycle of the system is significantly lower under the alternating normal force than the constant normal force, and the shapes of the limit cycle are different. Limit cycles exist in the system at excitation frequencies of 0.25 Hz, 0.5 Hz, and 1 Hz, but the numbers are different. This result shows that the system exhibits periodic stick-slip motion in these three states, but the motion patterns are different. There is no limit cycle at an excitation frequency of 2 Hz, and the motion trajectories are complex. Figure 5 exhibits that the motion state changes from stable periodic stick-slip vibration to irregular vibration as the frequency of the applied alternating force increases.

Figure 6 shows the tangential vibration acceleration signal and the RMS value of the acceleration when the system is in the stable phase of 50 s-55 s under the alternating normal force. At excitation frequencies of 0.25 Hz, 0.5 Hz, and 1 Hz, a phenomenon similar to that of applying a constant normal

force is observed, i.e., the tangential acceleration signal of the system exhibits relatively constant values interrupted by periodic peaks, and the system is in the stick-slip-stick vibration state. However, the difference is that the stick-slip vibration period becomes shorter, and the magnitude of the vibration reduces with an enlargement in the excitation frequency. The RMS values are similar at excitation frequencies of 0.25 Hz, 0.5 Hz, and 1 Hz (Fig. 6(b)), indicating similar vibration intensities of the system. In contrast, the tangential vibration acceleration signal of the system is more complex at an excitation frequency of 2 Hz, exhibiting a more chaotic vibration signal. Thus, the acceleration RMS value is significantly higher at 2 Hz than at the other three excitation frequencies, indicating that the vibration intensity and shape of the system are not solely stable stick-slip vibrations. Figure 6 indicates that increasing the excitation frequency of the alternating normal force causes the system to change from stable stick-slip vibration to unstable friction vibration.

4 The Stick-slip Vibration Characteristics Obtained From A Single-degree-of-freedom Theoretical Model

4.1 The stick-slip vibration characteristics of the system under a constant normal force

The first set of dynamic and static friction coefficients ($\mu_s = 0.4$, $\mu_k = 0.2$) is selected to research the stick-slip vibration characteristics of the system under a constant normal force. Figure 7 exhibits the phase diagram and bifurcation diagram under different constant normal forces. The external normal force gradually increases from 10 N to 40 N in steps of 5 N. As the constant normal force increases, stick-slip vibration appears in the system, and the amplitude of the limit cycle of the stick-slip vibration increases sequentially. It is manifest from the Fig. 7(b) that under the condition that the normal force keeps increasing, the balance point of the mass block produces a slight offset, whose value is calculated according to Eq. (6). Under the condition that the normal force keeps increasing, the offset and the amplitude of the mass block increase. The reason is that an increase in the normal force increases the maximum static friction force, inducing the system to generate a greater spring force to get over the static friction. The force ultimately promotes an increase in the adhesion time of the mass block, which stores and releases more energy in a single cycle.

{x_s}={\mu _k}{F_N}{\text{/}}{k_1}
6

The differential equations of the system are solved by MATLAB's ode45 solver. The initial parameter values are different; therefore, the system requires a different number of steps to reach a stable state. In this paper, the duration of each calculation is 100 πs, and the results of the first 300 s are shown in the graph. Only the data after t_1 (62.8 s) are selected for the frequency-domain analysis to prevent an influence of the initial value on the analysis of the system motion state. Figure 8 exhibits the time-domain and frequency-domain signals of the stick-slip vibration of the friction system under normal forces of 20 N and 25 N.

Under a constant normal force, the time-velocity curve of the mass shows a constant single-period motion state, and as the normal force increases, the amplitude and period of the system vibration increase. The frequency spectrum of the vibration velocity in $t_1 \sim 300$ s exhibits that the fundamental frequency of the system response reduces with an increase in the normal force. When the normal force is 20 N (25 N), the system produces a multi-order harmonic response with a fundamental frequency of 0.0855 Hz (0.0738 Hz). Table 1lists the fundamental frequencies of the system responses under different constant normal forces. As the normal force increases, the fundamental frequency of the vibration response decreases, and the vibration period of the system increases.

Table 1
The basic frequency of the stick-slip vibration response of the friction system under different constant normal forces

Normal force / F_N	Response fundamental frequency	Normal force / F_N	Response fundamental frequency
10 N	0.1243 Hz	30 N	0.0661 Hz
15 N	0.1010 Hz	35 N	0.0583 Hz
20 N	0.0855 Hz	40 N	0.0505 Hz
25 N	0.0738 Hz	—	—

Figure 9 shows the displacement-velocity two-dimensional phase diagram of the mass motion, the three-dimensional phase-space diagram expanded according to the motion cycle (the polar diameter and polar angle of the two-dimensional polar coordinate system respectively represent the displacement and the motion period, and the Z axis represents the speed), and the Poincaré cross-section based on the projection of the three-dimensional phase-space trajectory on a plane with a polar angle of π and parallel to the Z-axis (O in the figure represents the pole of the polar coordinates, and θ represents the polar angle). The Poincaré cross-section diagram is used to distinguish the periodic motion, quasi-periodic motion, chaotic motion, and other motion behaviors of the system according to the dynamic differential equations of nonlinear systems. Under the constant normal force, the motion state of the system shows stable single-period stick-slip vibration. The two-dimensional phase diagram indicates a single-period limit cycle, which is expanded in the three-dimensional phase-space with only one motion trajectory; thus, only one point is shown in the Poincaré cross-section in Fig. 9(c). Therefore, under the constant forces of 20 N and 25 N, the masses exhibit single-period stick-slip motion.

4.2 The stick-slip vibration characteristics of the system under an alternating normal force

Figure 10 shows the bifurcation diagram of the displacement of the mass with the angular frequency of excitation at a median alternating normal force of $F_0 = 25$ N and an amplitude of $F_\omega = 5$ N. As the exciting angular frequency increases, the mass exhibits multiple motion states, such as chaos, single-period vibration, and multi-period vibration. The bifurcation diagram is divided into seven regions. In region 'I',

the movement state of the system is disordered; in regions 'II', 'IV', and 'VI', the system is in a single-period motion state; in regions 'III', 'V', and 'VII', the system exhibits multiple motion states, including single-period, multi-period, quasi-period, and chaos states. Non-classical bifurcation phenomena are observed near critical points, such as sudden boundary changes and jumps. For example, when the excitation angular frequency is 1.35 rad/s (the critical point of regions 'IV' and 'V'), the single-period motion state of the mass block suddenly changes.

Further, we discuss the stick-slip vibration characteristics of the friction system for different angular frequencies. An excitation angular frequency of $\omega = 0.27$ rad/s is selected in the chaotic stage, and $\omega =$ 0.5 rad/s is selected in the single-period stage, and $\omega = 0.69$ rad/s and $\omega = 1.65$ rad/s are chosen in the vibration stage.

Figure 11 displays the phase diagram, phase-space diagram, and Poincaré cross-section diagram of the stick-slip vibration of the friction system at different angular frequencies. At $\omega = 0.27$ rad/s, multiple limit cycles are observed in the phase diagram. As the calculation time increases, the number of limit cycles increases, and the phase-space trajectory becomes more chaotic. Multiple discrete points are observed, and the system is in chaotic stick-slip motion at this time. At $\omega = 0.5$ rad/s, the phase diagram exhibits a single-period limit cycle, the phase-space diagram has only one trajectory, and only one point is visible in the Poincaré cross-section diagram. Under this circumstances, the system is in a single-period stick-slip motion state. At $\omega = 0.69$ rad/s, the system is in a two-period vibration state. The phase diagram and phase-space diagram show an additional trajectory, and the Poincaré cross-section diagram exhibits two discrete points. At $\omega = 1.65$ rad/s, the Poincaré cross-section depicts a straight line, and the system is in a quasi-periodic stick-slip state.

Figure 12 shows the external excitation signal, vibration velocity signal, and fast Fourier transform (FFT) analysis results of the system for four excitation angular frequencies. The value of t_1 is the same in Fig. 12 and Fig. 8. In Fig. 12(c), the left Y-axis depicts the FFT results of the speed signal, and the right Y-axis shows the stress vibration frequency (dashed line). The friction system produces multiple main response frequencies at an excitation angular frequency of 0.27 rad/s and an excitation frequency of 0.0430 Hz. The highest response frequency of the system is 0.0725 Hz, and the vibration behavior of the mass block is complex. At 0.5 rad/s, the friction system produces a multi-order harmonic response with a fundamental frequency of 0.0796 Hz. At this time, the excitation frequency is consistent with the response frequency of the system with the highest energy, and the system is in a single-cycle stick-slip state (Fig. 10). At 0.69 rad/s, the excitation frequency is 1.5 times of the response frequency of the system with the highest energy. At this time, the system is in a two-period stick-slip state. At 1.65 rad/s, the excitation frequency is in keeping with the third-order vibration frequency component of the system's response fundamental frequency, and the system is in a quasi-periodic stick-slip motion state.

Further, we select an excitation angular frequency in each region in Fig. 10 and calculate the response frequency of the system with the highest energy. The frequency data is exhibited in Table 2. The excitation angular frequency of 0.67 rad/s in area 'III is greater than the highest response frequency but

less than the second-order response frequency of the system. The value is three-half of the main frequency of the highest response of the system. At this time, area 'III' is the transition area between the single-period stick-slip motion areas 'II' and 'IV'. In area 'IV', the excitation angular frequency is 1 rad/s, which is consistent with the second-order response frequency of the system. The system is in a single-period stick-slip state. In region 'V', the excitation angular frequency is 1.7 rad/s, which is consistent with the third-order response frequency of the system. However, Fig. 10exhibits that the system is in a multi-period stick-slip motion state at this time. In area 'VI', the excitation angular frequency is 2.25 rad/s, which is consistent with the fourth-order response frequency of the system; the system is still in a single-period stick-slip motion state. In area 'VII', the excitation angular frequency is 3.15 rad/s, which is equal to the fifth-order response frequency of the system. As the excitation frequency increases, the system goes through different vibration states, including single cycle, multi-period, quasi-period, and chaotic vibration states.

Table 2
Response frequency of the system for different excitation angular frequencies

	Area	Excitation angular frequency ω(rad/s)	Excitation angular frequency(Hz)	The main frequency with the highest energy(Hz)
Median force: 25 N Excitation amplitude: 5 N	I	0.20	0.0318	0.0732
	II	0.52	0.0828	0.0828
	III	0.67	0.1066	0.0720
	IV	1.00	0.1592	0.0796
	V	1.70	0.2706	0.0902
	VI	2.25	0.3581	0.0901
	VII	3.15	0.5013	0.1003

These results show that the condition of the system is chaotic vibration when the excitation magnitude is constant, the excitation frequency does not cause a harmonic response of the system, and the excitation frequency is not a multiple of the main frequency of the system with the highest energy response. When the excitation frequency causes a harmonic response of the system, the system is in a single-cycle motion state if the excitation frequency is in keeping with the main frequency of the system with the highest energy response or an even-order multiple (second-order, fourth-order) of the main frequency. The system can have various vibration states if the frequency is the same as the dominant frequency of the highest odd-order (third-order) of the system, or the excitation frequency is greater than the dominant frequency of the higher-order (fifth-order) response of the system.

Figure 13 shows the bifurcation diagram of the mass displacement with the excitation angular frequency for an excitation amplitude value of F_ω=10 N. Increasing the excitation amplitude increases the displacement extremum of the bifurcation diagram of the system, which agrees with the results in Fig. 7.

The bifurcation diagram is divided into three regions, and the main frequency of the system response for different excitation angular frequencies is analyzed. The results are listed in Table 3. In area 'I', the excitation angular frequency is 0.15 rad/s. This excitation frequency does not cause a harmonic response of the system and is less than the main frequency response of the system with the highest energy. The movement state of the system is disordered. In area 'II', the excitation frequency is in keeping with the dominant frequency of the system's highest energy response, and the system is in a single-cycle stick-slip state. Two excitation angular frequencies (1.35 rad/s and 4.15 rad/s) are selected in area 'III'. At 1.35 rad/s, the excitation frequency is equal to the third-order response frequency of the system, and at 4.15 rad/s, the excitation frequency is in keeping with the seventh-order response frequency of the system. In area 'III', the motion state of the system changes from a single cycle to two cycles and ultimately enters a chaotic motion state as the excitation angular frequency increases. These results indicate that an increase in the excitation amplitude of the alternating normal force increases the area where the system is in multiple vibration states; the system is more likely to be in a state of chaotic motion.

Table 3
Response frequency of the system for different excitation angular frequencies

	Area	Excitation angular frequency ω(rad/s)	Excitation angular frequency(Hz)	The main frequency with the highest energy(Hz)
Median force: 25 N Excitation amplitude: 10 N	I	0.15	0.0239	0.0743
	II	0.55	0.0875	0.0875
	III	1.35	0.2149	0.0716
		4.15	0.6605	0.1247

The influence of the excitation amplitude value on the system motion state is analyzed for an excitation angular frequency of 0.5 rad/s. The bifurcation diagram of the mass displacement response is shown in Fig. 14. The bifurcation graph is divided into two regions. In region 'I', the system is in a multi-period stick-slip motion state, and the excitation frequency does not cause a higher energy response frequency of the system. In region 'II', the system is in a single-period stick-slip motion status, and the excitation frequency is in keeping with the response frequency of the system with the highest energy (see Table 4for the details).

Table 4
Response frequency of the system for different excitation amplitudes

	Area	Excitation amplitude F_ω(N)	Excitation frequency ω(Hz)	The main frequency with the highest energy(Hz)
Median force: 25 N	I	0.8	0.0796	0.0756
Excitation angular frequency: 0.5 rad/s	II	5.0	0.0796	0.0796
		10.0	0.0796	0.0796

Figure 15 exhibits the bifurcation diagram of the displacement response of the mass with the excitation amplitude at an excitation angular frequency of 1.65 rad/s. Similarly, the bifurcation graph is divided into three regions. The vibration form of the friction system is more complex for the excitation angular frequency of 1.65 rad/s than of 0.5 rad/s. In area 'I', the system is in a state of multi-period stick-slip motion. At this time, the external excitation frequency does not cause a multi-order harmonic response of the system and a higher energy response of the main frequency. In area 'II', the system is in a single-period stick-slip state, and the excitation frequency is equal to the fourth-order response frequency of the system. The displacement response of the mass block undergoes abrupt changes and increases at the critical points of regions 'II' and 'III'. In area 'III', the system is in a variety of vibration states prior to a normal force of 13.1 N. Subsequently, the system begins to bifurcate into two motion states, which can be approximated as a combination of two multi-period motions.

Different excitation amplitude values in area 'III' are chosen to calculate the response frequency of the system, as listed in Table 5. A state of motion exists where the excitation frequency stimulates the harmonic response of the system and is in keeping with the third-order response frequency. A harmonic response whose excitation frequency does not affect the system is also observed, resulting in a state of motion in keeping with the highest response frequency of the system. In addition, the friction system also has a two-period-like motion state in which two multi-period motions are combined, and the excitation frequency of the system is in keeping with the second-order response frequency of the system. At the same excitation amplitude, increasing the excitation frequency complicates the system's vibration form, and it becomes more difficult to transition to a single-period stick-slip state.

Table 5
Response frequency of the system for different excitation amplitudes

	Area	Excitation amplitude F_ω(N)	Excitation frequency ω(Hz)	The main frequency with the highest energy(Hz)
Median force: 25 N	I	1.0	0.2626	0.1472
Excitation angular frequency: 1.65 rad/s	II	2.8	0.2626	0.1313
	III	4.2	0.2626	0.0875
		5.1	0.2626	0.0875
		7.5	0.2626	0.0915
		8.5	0.2626	0.0875
		10.0	0.2626	0.2626
		11.5	0.2626	0.2626
		14.0	0.2626	0.1313

5 Influence Of An Alternating Normal Force On The System Vibration Characteristics For Different Friction Coefficients

5.1 The stick-slip vibration characteristics of the system under a constant normal force

Figure 16 exhibits the phase diagram and bifurcation diagram of the vibration response of the friction system under different constant normal forces for the coefficients $\mu_s = 0.4$ and $\mu_k = 0.1$. As the normal force increases, a slight deviation of the system equilibrium point occurs in the positive tangential direction, and the vibration amplitude of the mass limit cycle increases. In addition, the displacement of the mass shows a significant increase in the negative tangential direction (minimum point of displacement). It is manifest from Fig. 16(a) that the vibration form of the friction system does not change significantly when the constant normal force is changed. However, the motion form of the mass of the friction system changes after increasing the difference between the dynamic and static friction coefficients from ($\mu_s = 0.4$, $\mu_k = 0.2$) to ($\mu_s = 0.4$, $\mu_k = 0.1$). The reason is that an increment in the difference between DSFC increases the negative displacement of the mass block, affecting the compression state of the tangential spring as the mass block changes from the slip state to the stick state. When the external force generated by the spring is much greater than the dynamic friction force, the mass has

faster acceleration in the positive tangential direction, increasing the speed of the mass, as shown in Fig. 16(a).

Figure 17 exhibits the time-domain diagram and frequency spectrum diagram of the vibration velocity of the friction system at normal forces of 20 N and 25 N. Increasing the difference between DSFC does not change the motion state; the system has the stick and slip motion states. At a normal force of 20 N (25 N), the system's vibration response frequency is a multi-order harmonic response with a fundamental frequency of 0.0738 Hz (0.0637 Hz). Figure 18 shows the phase diagram, phase-space diagram, and Poincaré cross-section diagram of the vibration response of the friction system under the two normal forces. The phase diagram exhibits a single limit cycle, and the phase-space diagram depicts a single motion trajectory, but the limit cycle and phase-space trajectory are slightly deformed. The Poincaré cross-section diagram shows only one discrete point.

5.2 The stick-slip vibration characteristics of the system under an alternating normal force

Figure 19 shows the bifurcation diagram of the vibration displacement response of the mass of the friction system with the excitation angular frequency for coefficients $\mu_s = 0.4$ and $\mu_k = 0.1$. The median force is $F_0 = 25$ N, and the excitation amplitude is F_ω=5 N. When the difference between DSFC ($\mu_s = 0.4$, $\mu_k = 0.1$) is increased, the vibration state of the system is similar to that at $\mu_s = 0.4$ and $\mu_k = 0.2$, exhibiting single-period, multi-period, quasi-period, and chaotic vibration states. However, the chaotic vibration range is significantly increased. When the excitation angular frequency is close to 0.5 rad/s, the system exhibits smaller and larger vibration amplitudes. When the excitation angular frequency is within the other ranges, the range of the vibration amplitude changes slightly. The excitation angular frequencies of 0.51 rad/s, 1.25 rad/s, and 3.98 rad/s are selected for further analysis.

Figure 20 shows the phase diagram, phase-space diagram, and Poincaré cross-section diagram of the mass motion of the friction system for excitation angular frequencies of 0.51 rad/, 1.25 rad/s, and 3.98 rad/s. At 0.51 rad/s, multiple limit cycles occur in the phase diagram, and the phase-space trajectory shows very chaotic conditions. The Poincaré cross-section diagram shows irregularly distributed points. Under this circumstances, the system is in a chaos vibration state. At 1.25 rad/s, there are three limit cycles in the phase diagram of the friction system; correspondingly, there are three motion trajectories in the phase-space diagram and three discrete points on the Poincaré cross-section diagram. At this time, the system is in a three-period vibration state. The vibration type of the friction system at 3.98 rad/s is similar to that at 0.51 rad/s. There are multiple limit cycles in the phase diagram, and the phase-space trajectory is chaotic. Multiple discrete points are randomly distributed in the Poincaré cross-section diagram, and the system is in a state of chaotic vibration.

Figure 21 shows the normal force time-domain diagram of the friction system, the vibration velocity time-domain signal, and the FFT analysis results for excitation frequencies of 0.51 rad/s, 1.25 rad/s, and 3.98 rad/s. The meaning of t_1 in Fig. 21 is consistent with that in Fig. 8, and the details of the graph in Fig.

21(c) are consistent with that in Fig. 8(c). At an excitation angular frequency of 0.51 rad/s, the excitation frequency does not cause a harmonic response of the system, and the system has multiple response main frequencies. At 1.25 rad/s, the excitation frequency stimulates a multi-order harmonic response of the system and is consistent with the third-order response frequency of the friction system. At 3.98 rad/s, although the excitation frequency stimulates a multi-order harmonic response of the system, it is equal to the high-order response of the system, and the vibration state of the system is disordered. Increasing the difference between the friction coefficients from ($\mu_s = 0.4$, $\mu_k = 0.2$) to ($\mu_s = 0.4$, $\mu_k = 0.1$) results in the deformation of the limit cycle of the mass movement and an increase in the range in which the system is in a state of chaotic vibration.

Figure 22 shows the bifurcation diagram of the displacement response of the mass block with the excitation amplitude at an excitation angular frequency of 0.5 rad/s. The bifurcation graph is decomposed into four sections: 'I', 'II', 'III', and 'IV'. In area 'I', the system diverges from a single cycle to multiple cycles and finally enters a chaotic state as the excitation amplitude enhances. The excitation amplitude values of 1.8 N, 2.8 N, and 3.6 N are chosen to calculate the response frequency of the system. In area 'I', the external excitation frequency does not cause a higher response frequency of the system (see Table 6), and the system remains in a state of chaotic motion. In area 'II', the system has a smaller vibration amplitude. The excitation amplitude values of 5.8 N, 6.9 N, and 7.8 N are chosen to calculate the response frequency of the system. At this time, the external excitation frequency does not produce a harmonic response and a higher energy response frequency (see Table 6) of the system. In area 'III', the system enters a single-cycle motion state, and the external excitation frequency is consistent with the response frequency of the system with the highest energy (see Table 6). As the excitation amplitude value further increases, the system bifurcates into a two-period motion state in area 'IV', and the external excitation frequency remains the same as the response frequency of the system with the highest energy. These results show that increasing the difference between DSFC increases the likelihood of the system being in a multi-period vibration state or chaotic motion state. When the excitation amplitude value is very large, the system may branch into a multi-period vibration state, even if the external excitation frequency is consistent with the main response frequency of the system with the highest energy.

Table 6
Main response frequency of the system for different excitation amplitudes

	Area	Excitation amplitude F_ω(N)	Excitation frequency(Hz)	The main frequency with the highest energy(Hz)
Median force: 25 N Excitation angular frequency: 0.5 rad/s	I	1.8	0.0796	0.0637
		2.8	0.0796	0.0637
		3.6	0.0796	0.0637
	II	5.8	0.0796	0.2188
		6.9	0.0796	0.0637
		7.8	0.0796	0.1591
	III	8.9	0.0796	0.0796
		10.5	0.0796	0.0796
		12.6	0.0796	0.0796
	IV	14.2	0.0796	0.0796

6 Conclusion

The experiments demonstrated that an alternating normal force changed the vibration state of the system. We selected two sets of dynamic and static friction coefficients and used a single-DoF model to investigate the influence of the normal force on the vibration characteristics of the system. The system had more abundant dynamic vibration characteristics under an alternating normal force than a constant normal force. Furthermore, the effects of different excitation amplitudes and excitation angular frequencies on the alternating normal force on the system's vibration characteristics were obtained. The main conclusions are as follows:

1. For both sets of dynamic and static friction coefficients, as the constant normal force increased, the vibration amplitude of the system, the amplitude of the limit cycle, and the adhesion time of the system increased. When the difference between DSFC was small, the system had a complete and clear limit cycle. Reducing the coefficient of dynamic friction led to an increase in the difference between DSFC, and the limit cycle of the system was deformed.

2. Under the influence of changing excitation angular frequency and excitation amplitude, the system might be in a single-period, multi-period, and chaotic stick-slip vibration state. When the external excitation frequency caused a harmonic response of the system and was consistent with the system's highest energy response frequency or coincided with the low-order even-order (second-order, fourth-order) main frequency, the system was in a single-cycle stick-slip vibration state. When the excitation frequency

was different from the system's highest energy response frequency, or when the excitation frequency was in keeping with the odd-order main frequency of the system, the system could enter various vibration states. In addition, when the excitation frequency and excitation amplitude were very too high, the system could enter multiple vibration states earlier.

3. Under the influence of changing excitation angular frequency and excitation amplitude, the system was more likely to enter a chaotic vibration state or period-doubling bifurcation state when there was a large difference between DSFC.

Declarations

Acknowledgements

The authors are grateful for the Independent Research Projects of State Key Laboratory of Traction Power (2020TPL-T06), the Financial Support of the National Natural Science Foundation of China (No. 51822508), and the Sichuan Province Science and Technology Support Program (No. 2020JDTD0012).

Data availability The data used in this research work are available from the authors by reasonably request.

Conflict of interest The authors declare that they have no conflict of interest.

References

1. Berger, E.J.: Friction modeling for dynamic system simulation. Appl. Mech. Rev. **55**, 535–577 (2002)
2. Kinkaid, N.M., O'Reilly, O.M., Papaclopoulos, P.: Automotive disc brake squeal. J. Sound Vibr **267**, 105–166 (2003)
3. Yang, Z.Y., Han, J.M., Li, W.J., Li, Z.Q., Pan, L.K., Shi, X.L.: Analyzing the mechanisms of fatigue crack initiation and propagation in CRH EMU brake discs. Eng. Fail. Anal. **34**, 121–128 (2013)
4. Lu, X.D., Zhao, J., Mo, J.L., Zhang, Q., Zhang, X., Zhou, Z.R.: Improvement of dynamical and tribological properties of friction systems by introducing parallel-grooved structures in elastic damping components. Compos. Struct. **192**, 8–19 (2018)
5. Massi, F., Berthier, Y., Baillet, L.: Contact surface topography and system dynamics of brake squeal. Wear **265**, 1784–1792 (2008)
6. Papinniemi, A., Lai, J.C.S., Zhao, J.Y., Loader, L.: Brake squeal: a literature review. Appl. Acoust. **63**, 391–400 (2002)
7. Sinou, J.-J., Lenoir, D., Besset, S., Gillot, F.: Squeal analysis based on the laboratory experimental bench "Friction-Induced Vibration and noisE at Ecole Centrale de Lyon" (FIVE@ECL). Mech. Syst. Signal Proc. **119**, 561–588: (2019)
8. Zhao, X.W., Grabner, N., von Wagner, U.: Avoiding creep groan: Investigation on active suppression of stick-slip limit cycle vibrations in an automotive disk brake via piezoceramic actuators. J. Sound Vibr

441, 174–186 (2019)

9. Xiang, Z.Y., Mo, J.L., Qian, H.H., Zhu, S., Chen, W.: The effect of the friction block installation direction on the tribological behavior and vibrational response of the high-speed train brake interface. Wear. **484**, 204049 (2021)
10. Lyu, H.M., Walsh, S.J., Chen, G.X., Zhang, L.J., Qian, K.C., Wang, L.: Analysis of friction-induced vibration leading to brake squeal using a three degree-of-freedom model. Tribol Lett. **65**, 105 (2017)
11. Lacerra, G., Bartolomeo, M.D., Milana, S., Baillet, L., Chatelet, E., Massi, F.: Validation of a new frictional law for simulating friction-induced vibrations of rough surfaces. Tribol Int. **121**, 468–480 (2018)
12. Bonnay, K., Magnier, V., Brunel, J.F., Dufrenoy, P., De Saxce, G.: Influence of geometry imperfections on squeal noise linked to mode lock-in. Int. J. Solids Struct. **75–76**, 99–108 (2015)
13. Li, Z.L., Ouyang, H.J., Guan, Z.Q.: Nonlinear friction-induced vibration of a slider-belt system. J. Vib. Acoust. -Trans ASME **138**, 041006 (2016)
14. Yoon, S.W., Shin, M.W., Lee, W.G., Jang, H.: Effect of surface contact conditions on the stick-slip behaviour of brake friction material. Wear **294**, 305–312 (2012)
15. Wei, D.G., Ruan, J.Y., Zhu, W.W., Kang, Z.H.: Properties of stability, bifurcation, and chaos of the tangential motion disk brake. J. Sound Vibr **375**, 353–365 (2016)
16. Armstrong, B., Dupont, P., Dewit, C.C.: A survey of models, analysis tools and compensation methods for the control of machines with friction. Automatica **30**, 1083–1138 (1994)
17. Rashid, A.: Overview of disc brakes and related phenomena-a review. Int. J. Vehicle Noise Vib. **10**, 257–301 (2014)
18. Wang, X.C., Mo, J.L., Ouyang, H.J., Wang, D.W., Chen, G.X., Zhu, M.H., Zhou, Z.R.: Squeal noise of friction material with groove-textured surface: an experimental and numerical analysis. J. Tribol - Trans ASME **138**, 021401 (2016)
19. Hoffmann, N., Fischer, M., Allgaier, R., Gaul, L.: A minimal model for studying properties of the mode-coupling type instability in friction induced oscillations. Mech. Res. Commun. **29**, 197–205 (2002)
20. Giannini, O., Akay, A., Massi, F.: Experimental analysis of brake squeal noise on a laboratory brake setup. J. Sound Vibr **292**, 1–20 (2006)
21. Lima, R., Sampaio, R.: Parametric analysis of the statistical model of the stick-slip process. J. Sound Vibr **397**, 141–151 (2017)
22. Du, Z.W., Fang, H.B., Zhan, X., Xu, J.: Experiments on vibration-driven stick-slip locomotion: A sliding bifurcation perspective. Mech. Syst. Signal Proc. **105**, 261–275: (2018)
23. Capozza, R., Rubinstein, S.M., Barel, I., Urbakh, M., Fineberg, J.: Stabilizing stick-slip friction. Phys. Rev. Lett. **107**, 024301 (2011)
24. Woodhouse, J.: The acoustics of the violin: a review. Rep. Prog Phys. **77**, 115901 (2014)
25. He, B.B., Ouyang, H.J., He, S.W., Ren, X.M.: Dynamic analysis of integrally shrouded group blades with rubbing and impact. Nonlinear Dyn. **92**, 2159–2175 (2018)

26. Bettella, M., Harrison, M.F., Sharp, R.S.: Investigation of automotive creep groan noise with a distributed-source excitation technique. J. Sound Vibr **255**, 531–547 (2002)
27. Jearsiripongkul, T., Hochlenert, D.: Disk brake squeal: modeling and active control. 2006 IEEE Conference on Robotics, Automation and Mechatronics. (2006)
28. Wang, B.J., Wang, Z.Y., Ren, F.S.: Dynamic model and quantitative analysis of stick-slip vibration in horizontal well. Shock Vib. 2020, 8831111 (2020)
29. Guo, S., Xia, Y., Wei, X.Q., Zhou, Q.: Investigation on the stable and stick-slip crack propagation behaviors in double cantilever beam test. J. Adhes. **96**, 1198–1218 (2020)
30. Zhang, Z.G., Duan, N.Y., Lin, C.G., Hua, H.X.: Coupled dynamic analysis of a heavily-loaded propulsion shafting system with continuous bearing-shaft friction. Int. J. Mech. Sci. **172**, 105431 (2020)
31. Zhou, X.P., He, Y., Shou, Y.D.: Experimental investigation of the effects of loading rate, contact roughness, and normal stress on the stick-slip behavior of faults. Tectonophysics **816**, 229027 (2021)
32. Ostapchuk, A.A., Morozova, K.G.: On the mechanism of laboratory earthquake nucleation highlighted by acoustic emission. Sci. Rep. **10**, 7245 (2020)
33. Popp, K., Stelter, P.: Stick-slip vibrations and chaos. Philos. Trans. R Soc. A **332**, 89–105 (1990)
34. VanDeVelde, F., DeBaets, P.: Mathematical approach of the influencing factors on stick-slip induced by decelerative motion. Wear **201**, 80–93 (1996)
35. Ozaki, S., Hashiguchi, K.: Numerical analysis of stick-slip instability by a rate-dependent elastoplastic formulation for friction. Tribol Int. **43**, 2120–2133 (2010)
36. Elmaian, A., Gautier, F., Pezerat, C., Duffal, J.M.: How can automotive friction-induced noises be related to physical mechanisms? Appl. Acoust. **76**, 391–401 (2014)
37. Li, Z.L., Ouyang, H., Guan, Z.Q.: Friction-induced vibration of an elastic disc and a moving slider with separation and reattachment. Nonlinear Dyn. **87**, 1045–1067 (2017)
38. Pascal, M.: Sticking and nonsticking orbits for a two-degree-of-freedom oscillator excited by dry friction and harmonic loading. Nonlinear Dyn. **77**, 267–276 (2014)
39. Wei, D.G., Song, J.W., Nan, Y.H., Zhu, W.W.: Analysis of the stick-slip vibration of a new brake pad with double-layer structure in automobile brake system. Mech. Syst. Signal Proc. **118**, 305–316: (2019)
40. Lee, S.M., Shin, M.W., Lee, W.K., Jang, H.: The correlation between contact stiffness and stick-slip of brake friction materials. Wear **302**, 1414–1420 (2013)
41. Chandiramani, N.K., Srinivasan, K., Nagendra, J.: Experimental study of stick-slip dynamics in a friction wedge damper. J. Sound Vibr **291**, 1–18 (2006)
42. Park, C.W., Shin, M.W., Jang, H.: Friction-induced stick-slip intensified by corrosion of gray iron brake disc. Wear **309**, 89–95 (2014)
43. Dong, C.L., Shi, L.C., Li, L.Z., Bai, X.Q., Yuan, C.Q., Tian, Y.: Stick-slip behaviours of water lubrication polymer materials under low speed conditions. Tribol Int. **106**, 55–61 (2017)

44. Wang, X.C., Mo, J.L., Ouyang, H., Huang, B., Lu, X.D., Zhou, Z.R.: An investigation of stick-slip oscillation of Mn-Cu damping alloy as a friction material. Tribol Int. **146**, 106024 (2020)
45. Fuadi, Z., Adachi, K.: Stiffness effect on low-frequency stick-slip motion generated on a simple caliper-slider experimental model. Appl. Mech. Mater. **758**, 57–62 (2015)
46. Rusli, M., Fesa, M.H., Dahlan, H., Bur, M.: Squeal noise analysis using a combination of nonlinear friction contact model. Int. J. Automot. Mech. Eng. **17**, 8160–8167 (2020)
47. Wang, X.C., Huang, B., Wang, R.L., Mo, J.L., Ouyang, H.J.: Friction-induced stick-slip vibration and its experimental validation. Mech. Syst. Signal Proc. **142**, 106705: (2020)
48. Liu, N.Y., Ouyang, H.J.: Friction-induced vibration considering multiple types of nonlinearities. Nonlinear Dyn. **102**, 2057–2075 (2020)
49. Krallis, M., Hess, D.P.: Stick-slip in the presence of a normal vibration. Lubr Sci. **8**, 205–219 (2002)
50. Papangelo, A., Ciavarella, M.: Effect of normal load variation on the frictional behavior of a simple Coulomb frictional oscillator. J. Sound Vibr **348**, 282–293 (2015)
51. Pasternak, E., Dyskin, A., Karachevtseva, I.: Oscillations in sliding with dry friction. Friction reduction by imposing synchronised normal load oscillations. Int. J. Eng. Sci. **154**, 103313 (2020)
52. Xiang, Z.Y., Mo, J.L., Ouyang, H.J., Massi, F., Tang, B., Zhou, Z.R.: Contact behaviour and vibrational response of a high-speed train brake friction block. Tribol Int. **152**, 106540 (2020)
53. Karnopp, D.: Computer simulation of stick-slip friction in mechanical dynamic systems. J. Dyn. Syst. Meas. Control **107**, 100–103 (1985)

Figures

Figure 1

The test device; (a) photo and (b) schematic diagram

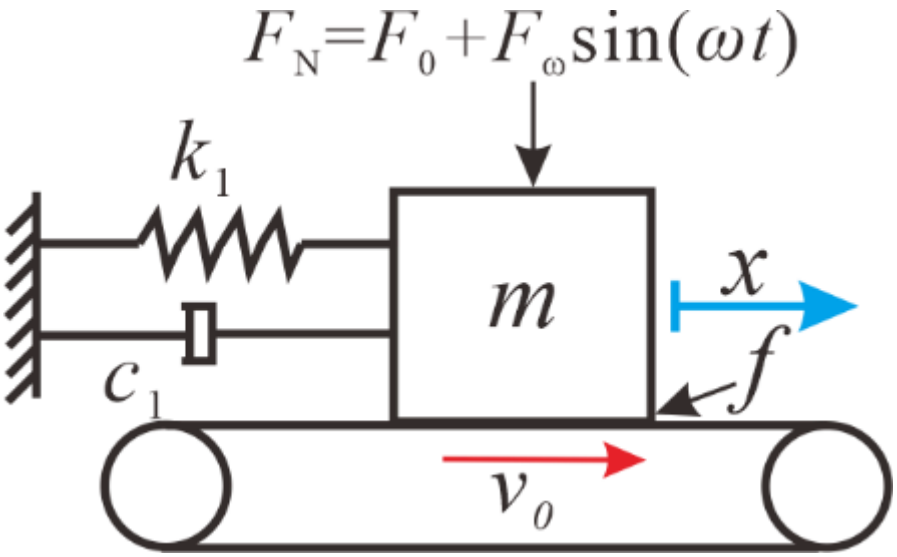

Figure 2

The single-DoF mathematical model

Figure 3

The phase diagram of the system under a constant force (a) 160 N, (b) 180 N, (c) 200 N

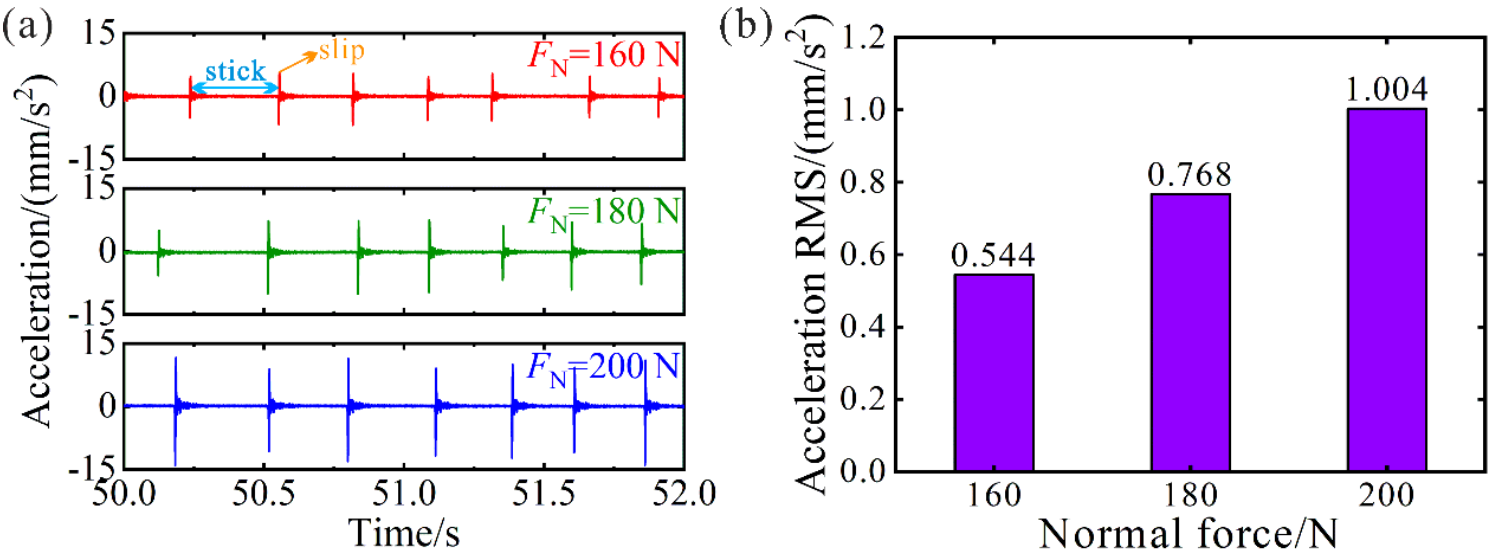

Figure 4

(a) Acceleration signal and (b) acceleration RMS value of the system under a constant force

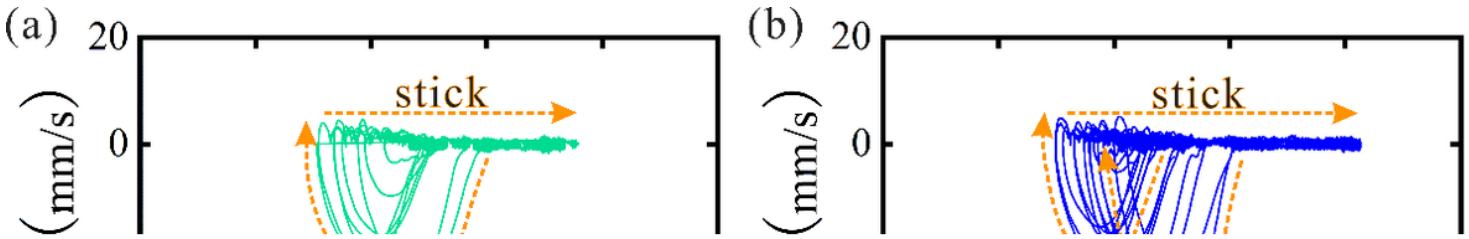

Figure 5

The phase diagram of the system under an alternating force (a) 0.25 Hz, (b) 0.5 Hz, (c) 1 Hz, (d) 2 Hz

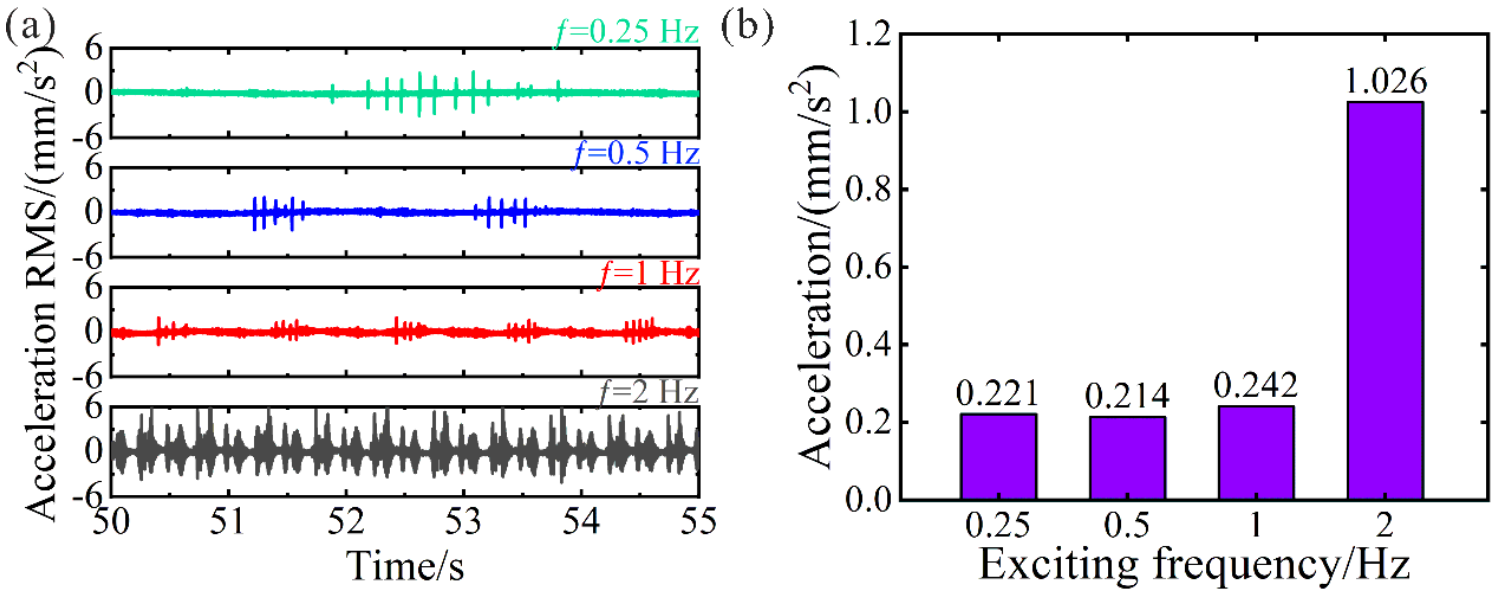

Figure 6

(a) Acceleration signal and (b) acceleration RMS value of the system under the alternating force

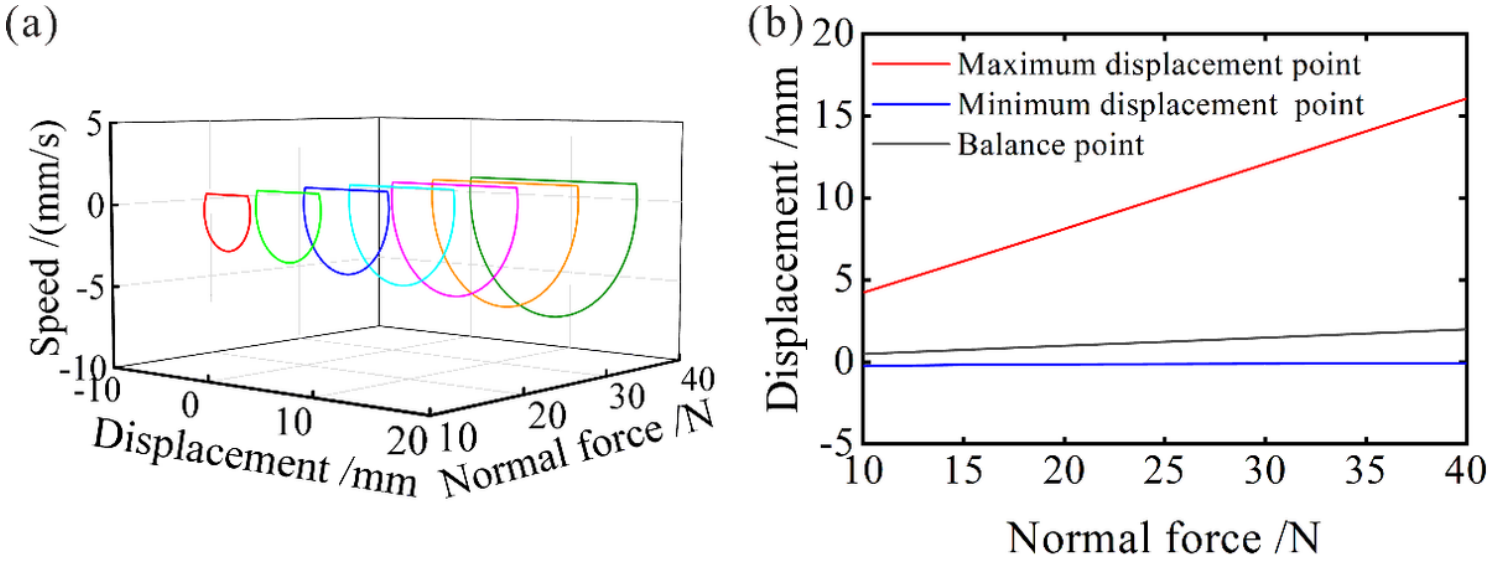

Figure 7

(a) Phase diagram and (b) bifurcation diagram of the system under different constant forces

Figure 8

(a) Vibration velocity time-domain signal and (b) FFT analysis results of the friction system under constant forces of 20 N and 25 N

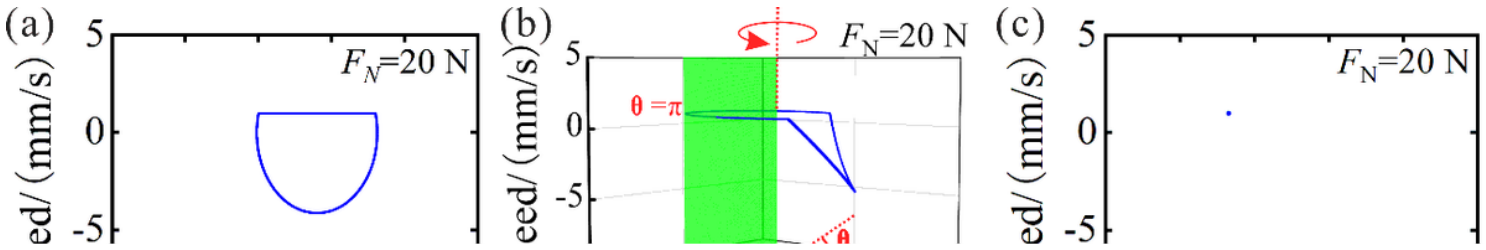

Figure 9

(a) Phase diagram, (b) phase-space diagram, and (c) Poincaré cross-section diagram of the system under different normal forces

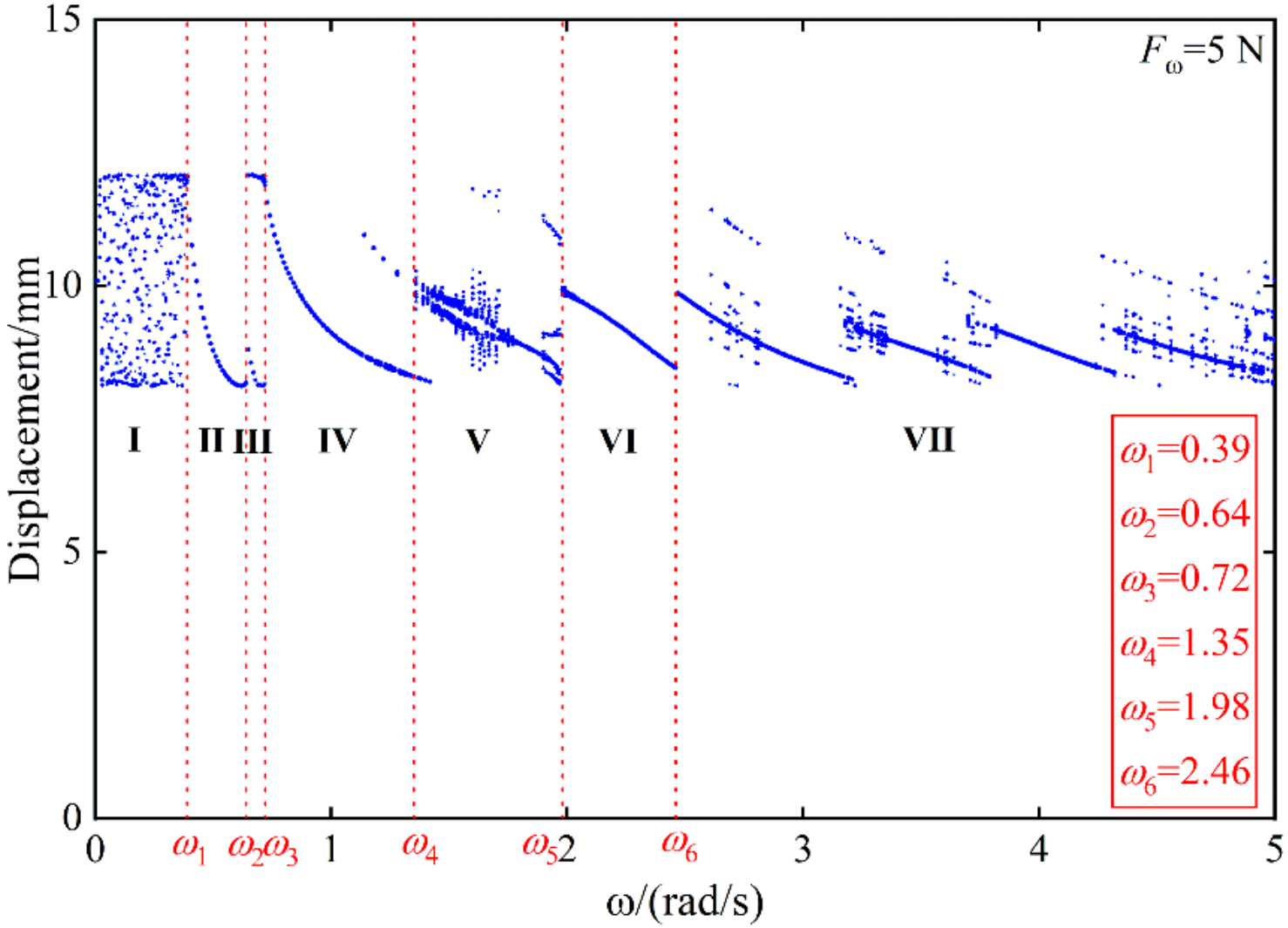

Figure 10

Bifurcation diagram of the system displacement with the excitation angular frequency at an excitation amplitude of 5 N

Figure 11

(a) Phase diagram, (b) phase-space diagram, and (c) Poincaré cross-section diagram of the system for different excitation angular frequencies

Figure 12

(a) Normal force time-domain diagram, (b) velocity time-domain diagram, and (c) frequency spectrum diagram of the system for different excitation angular frequencies

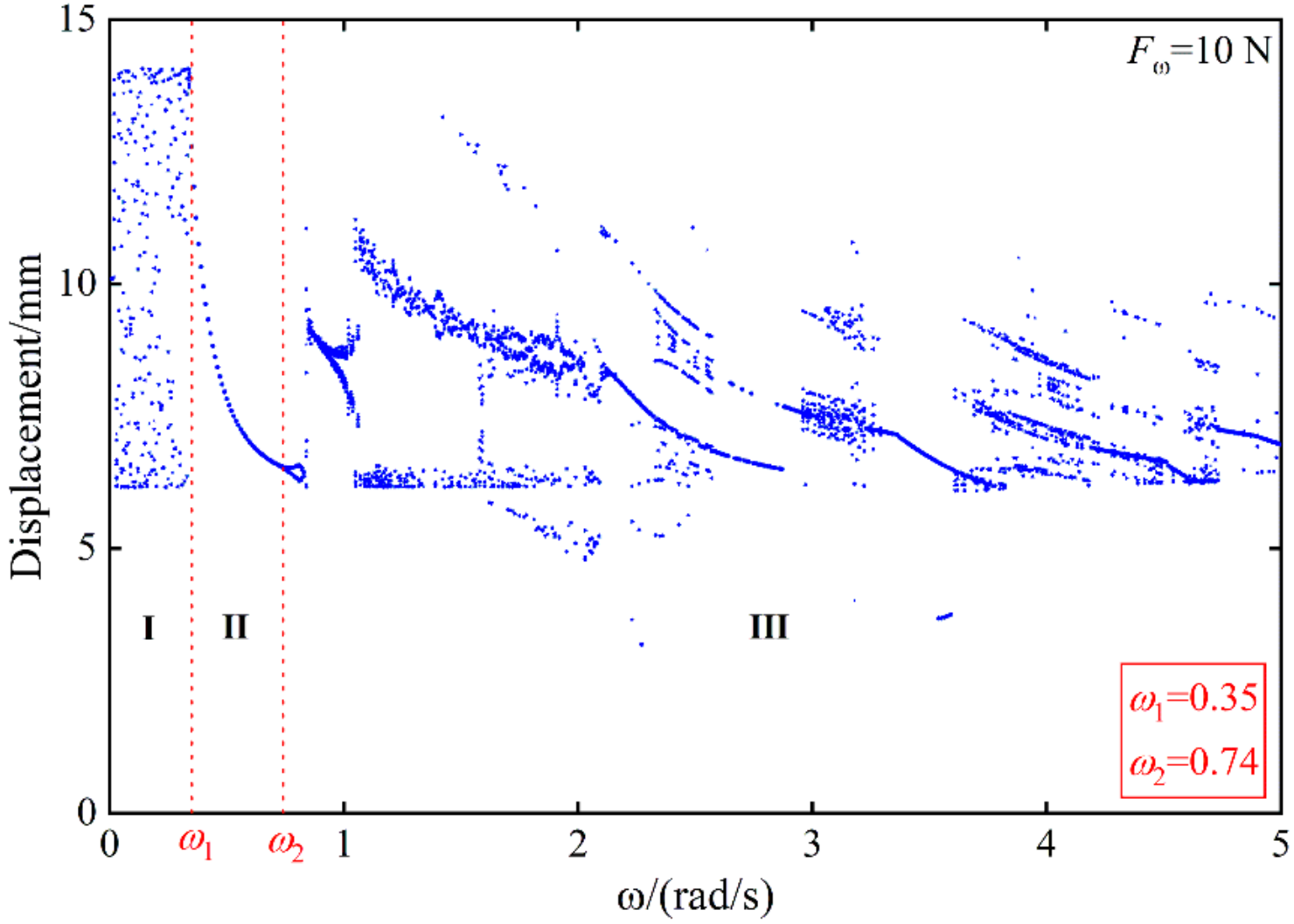

Figure 13

Bifurcation diagram of the system displacement with the excitation angular frequency at an excitation amplitude of 10 N

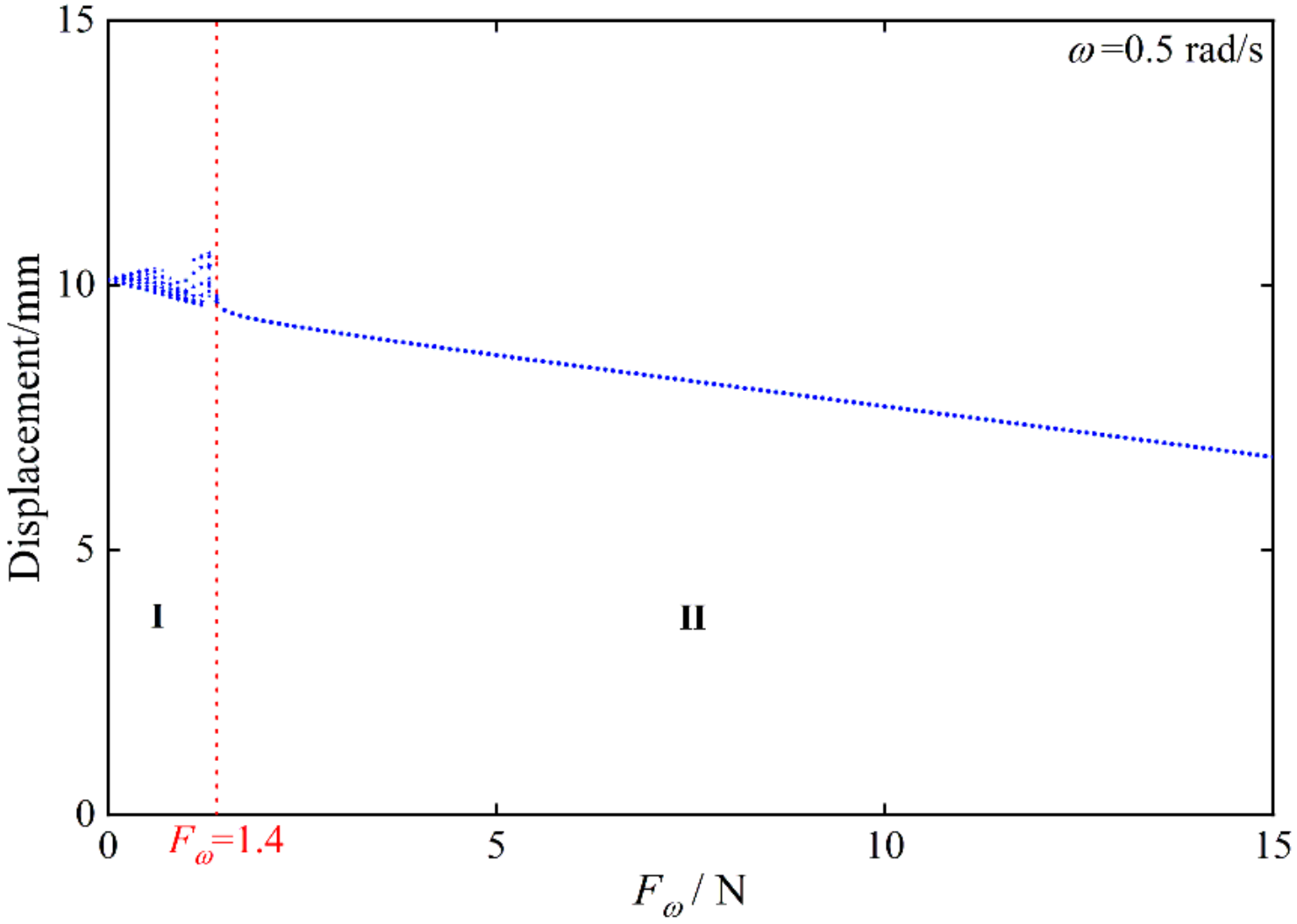

Figure 14

Bifurcation diagram of the system displacement with the excitation amplitude value at an excitation angular frequency of 0.5 rad/s

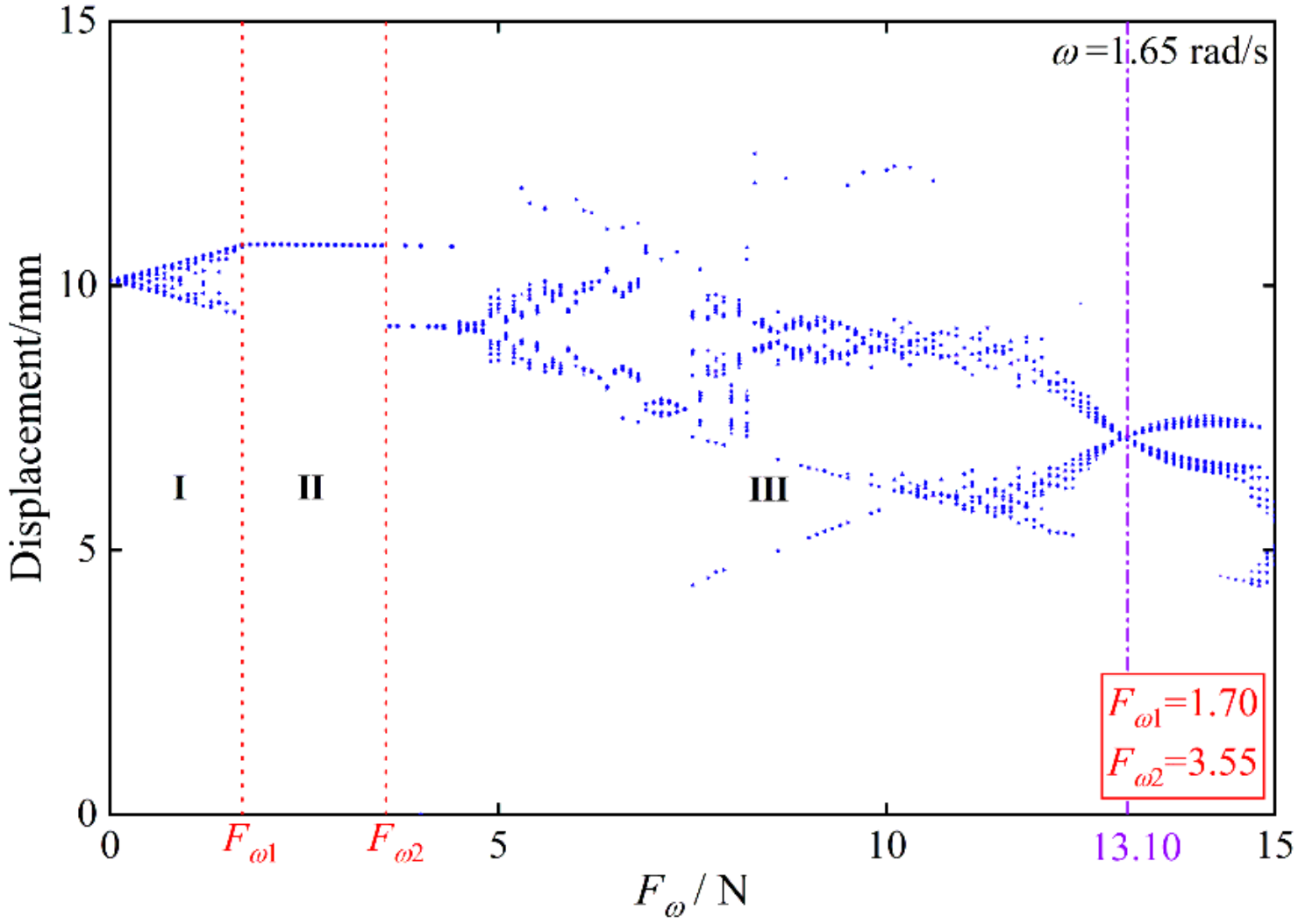

Figure 15

Bifurcation diagram of the system displacement with the excitation amplitude at an excitation angular frequency of 1.65 rad/s

Figure 16

(a) Phase diagram and (b) bifurcation diagram of the system vibration response under different constant normal forces

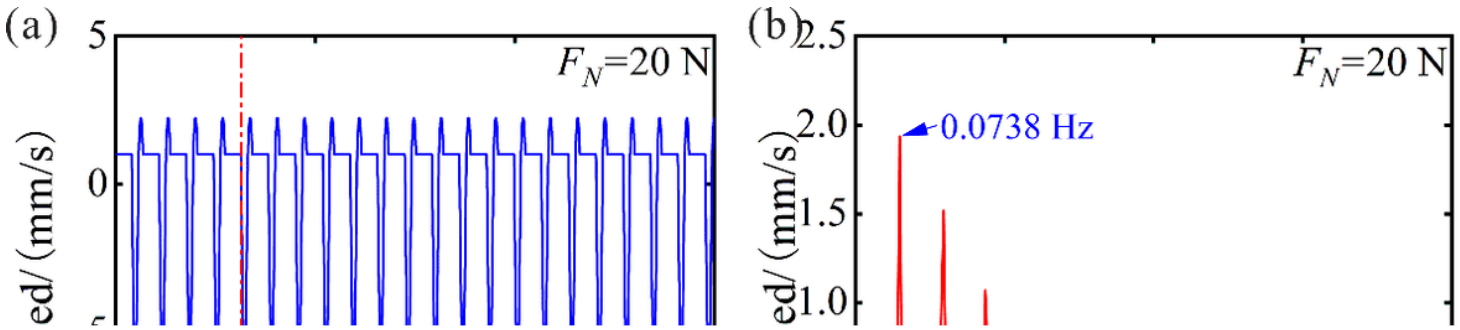

Figure 17

(a) Time-domain diagram and (b) frequency spectrum diagram of the system vibration response under a constant normal force

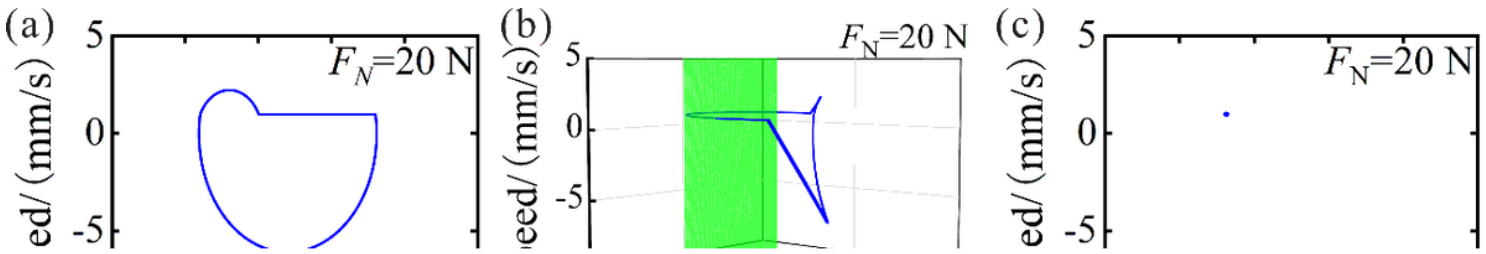

Figure 18

(a) Phase diagram, (b) phase-space diagram, and (c) Poincaré cross-section diagram of the system under a constant normal force

Figure 19

Bifurcation diagram of the vibration displacement of the friction system with the excitation angular frequency at an excitation amplitude of 5 N

Figure 20

(a) Phase diagram, (b) phase-space diagram, and (c) Poincaré cross-section diagram of the system for different excitation angular frequencies

Figure 21

(a) Normal force time-domain diagram, (b) velocity time-domain diagram, and (c) frequency spectrum diagram of the system for different excitation angular frequencies

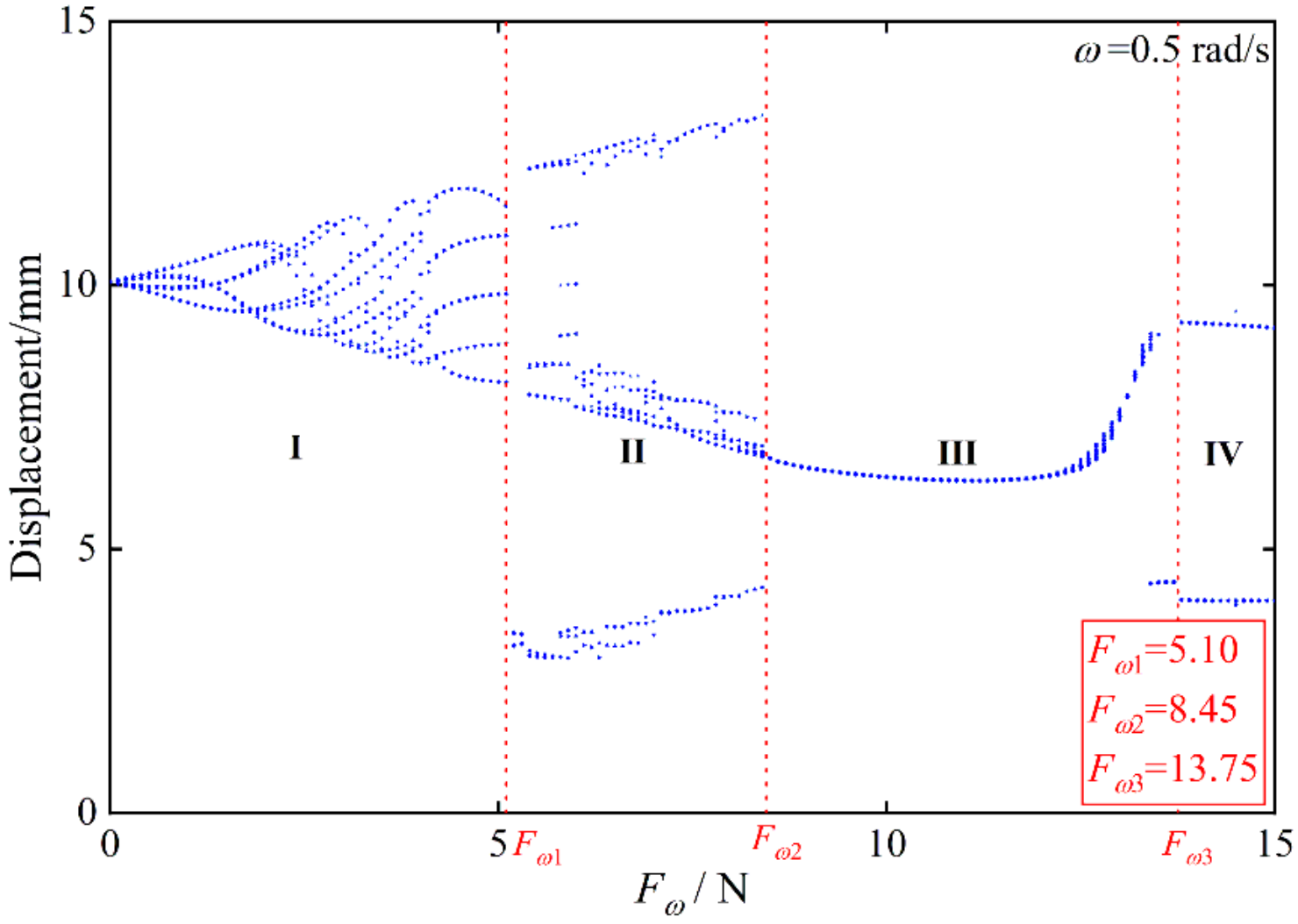

Figure 22

Bifurcation diagram of the system displacement with the excitation amplitude at an excitation angular frequency of 0.5 rad/s